RSC Advances

ROYAL SOCIETY OF CHEMISTRY

www.rsc.org/advances

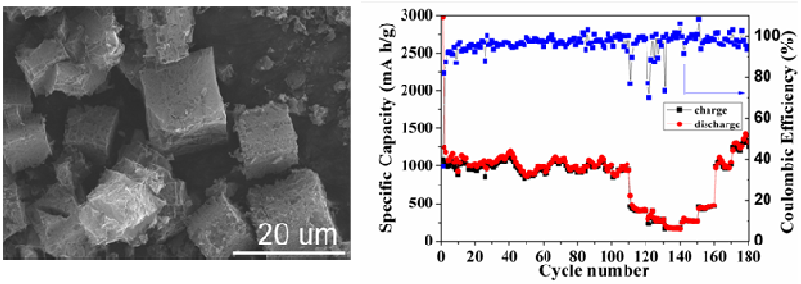

3D porous carbon derived by the MOFs with an excellent performance of 1015 mAh g^{-1} after 100 cycles for LIBs.

Facile Synthesis of Three-dimensional Porous Carbon with High Surface Area by Calcining Metal−Organic Framework for Lithium ion Batteries Anode Materials

Li Zuo, Shouhui Chen, Jiafeng Wu, Li Wang, Haoqing Hou and Yonghai Song*

College of Chemistry and Chemical Engineering, Jiangxi Normal University, 99 Ziyang Road, Nanchang 330022, China.

* Corresponding author: Tel/Fax: +86 791 88120862. E-mail: yhsonggroup@hotmail.com (Y. Song).

Abstract

A simple and convenient approach to prepare three-dimensional (3D) porous carbon with high surface areas of 1880 m^2 g^{-1} as anode materials for lithium ion battery (LIBs) was developed by calcining the $Zn_4O(BDC)_3$ (MOF-5, BDC = 1,4-benzenedicarboxylate) at 900 ℃ for 1 h. The resulted 3D porous carbon released an initial discharge of 2983 mA h g^{-1} and charge of 1084 mA h g^{-1} at a current density of 100 mA g^{-1}. The as-prepared porous carbon materials still maintained a high specific capacity of 1015 mA h g^{-1} after 100 cycles. The 3D porous carbon materials also exhibited superior cyclic stability and reversible capacity, making it a promising anode material and a good matrix material for LIBs.

1. Introduction

As the demand for low consumption and high energy density increased, lithium ion batteries (LIBs) have attracted more and more attentions due to its small volume, light quality, low self-discharge, environment friendly, high specific capacity, long cycle life, high operating voltage, wide temperature window and without ‘‘memory effect’’.[1-4] Recently, more attentions for the research of LIBs were focused on the development of excellent anode materials. Carbon materials are one of widely used anode materials for LIBs owing to its good chemical resistance and thermal stability. However, the traditional graphite has a capacity of only 372 mA h g^{-1},[2] which cannot meet the demands in modern society.

Porous carbon might be superior to traditional graphite because its open porous structure could provide more active sites, moderate electrical conductivity, a large surface areas as well as a very short diffusion pathway for Li^+ transfer.[5,6] The pore could also act as a buffer for the large volume change during the process of charge and discharge to delay capacity fading.[7-12] Therefore, porous carbons with ordered structure and high surface areas might exhibit large irreversible capacity and superior cyclic stability. Porous carbon materials can be synthesized through different ways, such as soft template method,[13-15] hard template method,[16-19] nanocasting method[20-23] and so on. The hard template method is one of the widely used ways to gain ordered porous carbon materials. The hard template contains preformed porous solids, anodic aluminum oxide membranes, assemblies of colloidal particles, biotemplates and others with ordered rigid structures unlike soft template.[10] As an kind of emerging materials, metal–organic framework (MOF) have attracted a lot of interests because of their versatile functionalities and tunable porosities,[24] which has also been employed as a hard template to obtain porous carbon. Liu et al. prepared the porous carbon for supercapacitor by polymerizing and then carbonizing carbon precursor of furfuryl alcohol embedded in a porous

MOF-5 ($Zn_4O(BDC)_3$, BDC = 1,4-benzenedicarboxylate) template, showing a almost constant specific capacitance of 100 F/g at 5 mV/s.[25] Hierarchically porous carbon-coated ZnO quantum dots (QDs) were synthesized by a one-step controlled pyrolysis of the MOF-5 for LIBs showing the superior performance mainly due to the ZnO QDs.[26] In this work, we found that pure 3D porous carbon derived from MOF-5 could also show an excellent performance after removal off the ZnO QDs.

In this paper, by using the MOF-5 as template to synthesize stable porous carbon materials for LIBs, its performance is also superior to other traditional carbon and some composed materials, making it a promising anode material and a good matrix material for LIBs. This method are simple and worth exploring.

2. Experiment section

2.1. Reagents and materials

The zinc nitrate hexahydrate and terephthalic acid (H_2BDC) were obtained from Aladdin. Dimethyl formamide (DMF) was purchased from Guangdong Xilong Chemical Reagent Factory (Guangdong, China). Other reagents were purchased from Beijing Chemical Reagent Factory (Beijing, China). Carbon black (Kaisai Shanghai Chemicals), polyvinylidene fluoride (PVDF, Lefu Shanghai Chemicals), metallic Li foil (0.6 mm thickness, 99.9%, Zhongneng Tianjin Company) and copper foil (10 μm thickness, Jiayuan Guangzhou Company) were used without further treatment. Other chemicals used in this study are analytical grade. Ultra-pure water purified by a Millipore-Q System (18.2 MΩ cm) was used.

2.2 Synthesis of 3D porous carbon materials

MOF-5 was synthesized according to the literature.[27,28] Briefly, 5.45 g of zinc nitrate hexahydrate (18.3 mmol) and 1.0 g of H_2BDC (6 mmol) were dissolved in 150 mL of DMF. The two solutions

were mixed in equal volume, and then the mixed solution was transferred into a beaker, and heated to 120 ℃ for 4 h. Finally, the crude product was washed with DMF several times and then dried at room temperature. MOF-5 was placed in a ceramic boat and was then transferred into a horizontal quartz tube and calcined in the horizontal tube furnace. The thermolysis was performed under a N_2 atmosphere with a heating rate of 5 ℃ min^{-1} from room temperature to 900 ℃ for 1 h, followed by natural cooling to room temperature. Finally, the black 3D porous carbon was obtained. The preparation procedure was illustrated in Scheme 1.

2.3. Characterization

Scanning electron microscopy (SEM) images were taken by using a XL30 ESEM-FEG SEM at an accelerating voltage of 20 kV equipped with a Phoenix Energy Dispersive Spectrometer (EDS) to study the product morphology. X-ray powder diffraction (XRD) data were collected on a D/Max 2500 V/PC X-ray powder diffractometer using Cu Kα radiation (λ=1.54056 Å, 40 kV, 200 mA). Thermogravimetric analysis (TGA) was conducted on SDT 2960 with a heating rate of 5 ℃ min^{-1}, using an SDT 2960 instrument. Fourier transform infrared spectroscopy (FTIR) was obtained on a Perkin-Elmer Spectrome 100 spectrometer (Perkin-Elmer Company, USA). N_2 adsorption/desorption isotherms were measured at -196 ℃, using an ASAP 2020 instrument (Micromeritics). Before the experiments, the samples were degassed under vacuum at 150 ℃ for 3 h. The surface areas, pore volume and pore size distribution of the samples were determined based on the N_2 adsorption/desorption isotherm. Transmission electron microscopy (TEM) was carried out on a JEM-2010 (HR) microscope.

2.4. Electrochemical performance measurements

The working electrodes were made by a slurry coating procedure. The as-prepared samples were mixed with acetylene black and carboxymethyl cellulose in a weight ratio of 8:1:1 in N-methyl

pyrrolidinone to form homogeneous slurry and then were spread uniformly on copper foil which was acted as a current collector. The fabricated working electrodes were dried in oven at 60 ℃ for overnight, and then dried in a vacuum oven at 120 ℃ for 5 h. A celgard 2300 microporous polypropylene film was used as separator. The cells were assembled in an argon-filled glove box using Li foil as counter electrodes. The electrolyte was made of 1.0 M LiPF6 dissolved in a 1:1 (v/v) mixture of ethylene carbonate and dimethyl carbonate. Electrochemical impedance spectroscopy (EIS) was carried out with a CHI 760D electrochemical workstation (CH Instruments, Shanghai, China) using a conventional three-electrode system with Li metal as the counter and reference electrode, active materials as the working electrode. Other electrochemical experiment was carried out in two-electrode coin cells. The electrochemical discharge/charge tests of the samples were performed on a Neware BTS test system (Shenzhen, China) at voltage limits of 3.0~0.01 V versus Li/Li^+.

3. Results and discussion

The as-prepared MOF-5 was firstly characterized by SEM. As shown in Fig. 1a, the MOF-5 exhibited a very neat surface. The side length of cube was almost 10-30 μm. The high-magnification image (Inset of Fig. 1a) showed that it had a special gully structure. The EDS of MOF-5 was also shown in Fig. 1b and it clearly indicated that the MOF-5 mainly contained Zn, C and O elements

Fig. 1c presented the XRD pattern of MOF-5, which perfectly matched with the reported literature.[28] The diffraction peak at 9.4^o corresponded to the (220) crystalline planes of Zn_4O. Another characteristic peak at $2\theta = 6.9^o$ was probably due to disruption of periodicity induced by solvent molecules filled into the pores of MOF-5.[29,30] All the above data demonstrated perfect crystal MOF-5 was synthesized successfully.

Fig. 1d showed the TGA curve of MOF-5. As proved by previous document,[26] the MOF-5 was decomposed into ZnO and porous carbon at the temperature higher than 500 ℃. With temperature further increasing to higher than 800 ℃, ZnO was reduced into metallic Zn species. Subsequently Zn metal (boiling point 908 ℃) vaporized away along with the N_2 flow, forming porous carbon.[31] Although the boiling point of Zn was 908 ℃, Zn element was still vaporized to form the porous carbon when the temperature of the tubular furnace atmosphere was set to 900 ℃ due to inaccurate temperature controlling as shown by Fig. 1d. Therefore, the 3D porous carbon was obtained by calcining MOF-5 at 900 ℃ for 1 h.

"Here Fig. 1"

The resulted 3D porous carbon was characterized by SEM as shown in Fig. 2. It showed a cubic shape of 3D porous carbon with lot of defects. The side length of cube was almost 10-30 μm, too. Fig. 2b showed the high-magnification SEM image of 3D porous carbon, suggesting that the surface of cube has unique patterns composed of irregular gully and some pores. The SEM results obviously indicated that the 3D skeletal matrix could be well preserved during thermolysis. After removal off ZnO, many holes were formed and resulted in the 3D porous skeleton structure, which provided a connecting network to enhance the mass transfer and offered more active sites for embedding Li^+.

TEM was employed to explore the porous structure of 3D porous carbon as shown in Fig. 2c. It clearly revealed that many brightness and darkness on the fluffy 3D porous carbon and indicated the carbon material with different thickness. Besides, the high-magnification image (Fig. 2d) further confirmed the porous structure of as-prepared carbon material.

"Here Fig. 2"

The EDS of 3D porous carbon was also shown in Fig. 3a. After heating treatment, the major

element was C. The presence of O peak (0.53 keV) was probably due to the C–OH and oxygen adsorbed in the porous carbon, since the FTIR spectrum of 3D porous carbon (Fig. 3b) showed bands at 1629 cm^{-1} and 1388 cm^{-1}, which were attributed to the C=C stretching vibration and C–OH deformation vibration.[32] The small peak at 1.74 keV might result from the silicon substrate used for supporting porous carbon. The results indicated that pure porous carbon without ZnO was obtained by calcining MOF-5 at 900 ℃ for 1 h.

Fig. 3c presented the XRD patterns of 3D porous carbon. The diffraction peaks located at 23° and 44° was corresponding to the (002) and (101) diffraction planes of porous carbon (JCPDS No. 41−1487), respectively. The diffraction peak at 23 ° in the XRD pattern was attributed to the formation of graphite layers in the porous carbon.[14] The absence of other signal in the XRD pattern confirmed that the Zn element had been removed off completely.

Raman spectra played a significant role in the characterization of carbon materials. Fig. 3d showed the Raman spectra of 3D porous carbon. Obviously, two peaks were observed , which corresponded to the disordered structures of carbon materials (D band) and the C–C bond vibrations of carbon atoms with sp^2 electronic configuration (G band) in carbon structure, respectively. The appearance of D band and G band at the same time might be associated with the disordered graphite and ordered graphite in the porous carbon.

The 3D porous carbon was further analyzed by N_2 adsorption/desorption isotherms experiments. It was performed to examine surface areas and the pore size distribution of the 3D porous carbon. According to the Barrett-Joyer-Halenda model, the inset in Fig. 3e showed that as-prepared porous carbon has relatively broad mesopores with a maximum frequency near 14 nm. Based on the N_2 adsorption/desorption result in Fig. 3e, the 3D porous carbon exhibited a very high BET surface area of 1880 m^2 g^{-1}, the average pore size of 4.73 nm and a total pore volume of 2.22 cm^3 g^{-1},

indicating the 3D porous carbon not only provided mesoporous for Li^+ transfer but also possessed the high surface areas for Li^+ storage.

"Here Fig. 3"

The cyclic voltammograms of the 3D porous carbon electrodes at 0.2 mV/s over the voltage range from 0.01 to 3.00 V were shown in Fig. 4a. In general, the discharge process of the porous carbon could be divided into two main regions, negative and positive to 0.5 V vs. Li/Li^+. The region negative to 0.5 V was mainly due to the intercalation of Li^+ into the graphitic-type layers. The region positive to 0.5 V was attributed to the formation of the solid electrolyte interface (SEI) layer.[23] In this work, the peak located at 0.63 V in the first cycle might be attributed to the formation of SEI on the surface of porous carbon. Another two peaks at 1.4 and 1.7 V were mainly attributed to the reduction of surface species containing oxygen.[24,33,34] A broad peak at approximately 1.2 V was observed during the charge process. According to Frackowiak,[35] this behavior might partly be attributed to the interaction between the Li^+ and surface-oxygenated functional groups. The surface available for the adsorption was mainly located at the interstitial space between the adjacent pore walls and the empty spaces between 3D porous carbon.[36,37] Therefore, the 3D porous carbon exhibited superior electrochemical properties with respect to Li^+ insertion and extraction.

Fig. 4b presented the electrochemical charge/discharge curves of 3D porous carbon for the 1st, 2nd and 100th cycles at 100 mA g^{-1}. There was a long voltage plateaus in the first discharge step above 0.9 V for 3D porous carbon in the discharge curves of the first cycle, characteristic of the amorphous porous carbon.[38] The first charge/discharge curve of 3D porous carbon indicated the initial discharge and charge capacities of the 3D porous carbon at a 100 mA g^{-1} were 2983 and 1084 mA h g^{-1}, respectively. To our knowledge, the reversible capacity was much larger than that of most of carbon materials. The good performance might be attributed to the existence of plenty of

micropores (according to inset of Fig. 3e) in the porous carbon which acted as reservoirs for Li^+ storage.[39] The high irreversible capacity and low coulombic efficiency of porous carbon might be caused by the formation of SEI film and the irreversible Li^+ insertion associated with the hydroxyl groups and physically absorbed water on the surface of the carbon materials.[40] Actually, the formation of SEI film was very necessary. The SEI film prevented excessive solvent co-intercalation and also acted as a good Li^+ conductor to enable facile Li cycling. Further, the SEI film protected the LiC_x (charged graphite) which was a strong reducing agent from direct contacting with the solvents of the electrolyte and thereby suppressed the unwanted side reactions. In the second cycle, the coulombic efficiency of porous carbon was more than 80%. What's more, the capacity of 100th cycle could almost matches with the 2nd cycle, indicating excellent cycling performance. Therefore, the 3D porous carbon exhibited superior electrochemical properties with respect to Li^+ insertion and extraction.

"Here Fig. 4"

The charge/discharge cyclic performance of the 3D porous carbon evaluated at 100 mA g^{-1} in the voltage between 3.0 and 0.01 V was shown in Fig. 5a. The 3D porous carbon exhibited a very high specific capacity owing to multiple accessible sites for Li^+. The initial discharge and charge capacities of the 3D porous carbon at a 100 mA g^{-1} were 2983 and 1084 mA h g^{-1}, respectively. The bigger specific surface area and the more SEI film led to the big irreversible capacity. It was found that the capacity of 3D porous carbon was about 1015 mA h g^{-1} after 100 cycles in 100 mA g^{-1}, which was much higher than that of commercial graphite (372 mA h g^{-1}). Thus it was expected to replace graphite in industrial production. What's more, the 3D porous carbon exhibited an outstanding cycle performance. The high capacities of 3D porous carbon during the discharge and charge process might result from the ordered and loose porous structure and big surface area.

Rate performance of the 3D porous carbon might be important in commercial applications. As shown in Fig. 5b, the capacities of 3D porous carbon could recover back to 1324 mA h g^{-1} after the rate performance test, demonstrating the excellent recyclability of the as-prepared materials. At a high current rate, the 3D porous carbon exhibited highly reversible capacity (average of 173 mA h g^{-1} at 5 A g^{-1}) and excellent cycling stability in Li^+ storage and retrieval. The reason why it more than initial capacity of 1015 mA h g^{-1} was that the rate performance test made the battery activation completely. Therefore, the 3D porous carbon was suitable to be active anode materials for LIBs. And the capacity retention of the 3D porous carbon and high-rate capability was highly dependent on its morphology and porous structure.

"Here Fig. 5"

A comparison of the performance of our newly designed porous carbon with those already reported in literature was shown in Table 1. By way of comparison, it could be clearly seen that the 3D porous carbon materials presented high capacity and good cyclic stability. The unique porous structure and high surface area of the carbon materials provided more binding sites for Li^+ fully insertion. The 3D porous carbon materials could effectively alleviate the collapse of electrode material during the Li^+ insertion/extraction and avoid the rapid capacity fading. Furthermore, the 3D porous carbon derived from MOF-5 was superior to some porous carbon derived from other MOFs. Compared with porous carbon-coated ZnO QDs material,[26] the as-prepared porous carbon materials without ZnO could avoid the pollution of the waste batteries. The porous carbon obtained by using HCl to remove off ZnO showed a low capacity of 400 mA h g^{-1} only after 20 cycles at 75 mA g^{-1}.[26] In this work, porous carbon was prepared by calcining MOF-5 at high temperature directly, and the 3D skeletal matrix could be well preserved during carbonization and it showed good electrochemistry performance. The preparation process was much simple and convenient. It

was worth mentioning that the 3D porous carbon could not only be used as a single material but also served as a stable matrix to provide a source of porous electrode material.

"Here Table 1"

4. Conclusions

A simple method was developed to successfully synthesize the 3D porous carbon materials by calcining the MOF-5. The as-synthesized 3D porous carbon materials could act as a novel anode or matrix materials for LIBs. In this work, the 3D porous structure of the as-prepared carbon material not only provided more binding sites for Li^+ insertion/extraction but also provided the channels for charge and ionic transport. As a consequence, the as-prepared porous carbon exhibited a high reversible capacity (1015 mA h g^{-1} at 100th cycle), excellent cyclic performance and good rate capability. The strategy to prepare stable porous carbon materials by using the MOF as template will open up an opportunity for the development of LIBs. The strategy might be also extended to the synthesis of other porous carbon based on MOF.

Acknowledgements

This work was financially supported by National Natural Science Foundation of China (21165010, 21465014 and 21465015), Science and Technology Support Program of Jiangxi Province (20123BBE50104 and 20133BBE50008), Young Scientist Foundation of Jiangxi Province (20122BCB23011), Natural Science Foundation of Jiangxi Province (20142BAB203101), Young Scientist Foundation of Jiangxi Province (20122BCB23011), The Ministry of Education by the Specialized Research Fund for the Doctoral Program of Higher Education (20133604110002) and the Ground Plan of Science and Technology Projects of Jiangxi Educational Committee (KJLD14023).

References

1. V. Etacheri, R. Marom, R. Elazari, G. Salitra and D. Aurbach, *Energy Environ. Sci.* , 2011, **4**, 3243-3262.
2. L. Ji, Z. Lin, M. Alcoutlabi and X. Zhang, *Energy Environ. Sci.*, 2011, **4**, 2682-2699.
3. J. W. Long, B. Dunn, D. R. Rolison and H. S. White, *Chem. Rev.*, 2004, **104**, 4463-4492.
4. M. Winter and R. J. Brodd, *Chem. Rev.*, 2004, **104**, 4245-4270.
5. L. Ji and X. Zhang, *Electrochem. Commun.*, 2009, **11**, 1146-1149.
6. S. Xin, Y.-G. Guo and L.-J. Wan, *Acc. Chem. Res.*, 2012, **45**, 1759-1769.
7. T. Kyotani, T. Nagai, S. Inoue and A. Tomita, *Chem. Mater.*, 1997, **9**, 609-615.
8. C. Liang, K. Hong, G. A. Guiochon, J. W. Mays and S. Dai, *Angew. Chem. Int. Ed.*, 2004, **43**, 5785-5789.
9. T.-Y. Ma, L. Liu and Z.-Y. Yuan, *Chem. Soc. Rev.*, 2013, **42**, 3977-4003.
10. A. Vu, Y. Qian and A. Stein, *Adv. Eng. Mater.*, 2012, **2**, 1056-1085.
11. D.-W. Wang, F. Li, M. Liu, G. Q. Lu and H.-M. Cheng, *Angew. Chem. Int. Ed.*, 2008, **47**, 373-376.
12. H. Yamada, T. Hirai, I. Moriguchi and T. Kudo, *J. Power Sources*, 2007, **164**, 538-543.
13. C. Liang, Z. Li and S. Dai, *Angew.Chem., Int. Ed*., 2008, **47**, 3696-3717.
14. J. Lee, J. Kim and T. Hydeon, *Adv. Mater.*, 2006, **18**, 2073-2094.
15. Y. Wan, Y. Shi and D. Zhao, *Chem. Mater.*, 2008, **20**, 932-945.
16. T. F. Baumann and J. H. Satcher, *Chem. Mater.*, 2003, **15**, 3745-3747.
17. R. Ryoo, S. H. Joo and S. Jun, *J. Phys. Chem. B*, 1999, **103**, 7743-7746.
18. J. Lee, S. Yoon, T. Hyeon, S. M. Oh and K. B. Kim, *Chem.Commun*., 1999, 2177-2178.
19. F. Zhang, K.-X. Wang, G.-D. Li and J.-S. Chen, *Electrochem. Commun.*, 2009, **11**, 130-133.
20. X. Wang, C. Liang and S. Dai, *Langmuir*, 2008, **24**, 7500-7505.
21. F. Zhang, Y. Meng, D. Gu, Y. Yan, Z. Chen, B. Tu and D. Zhao,*Chem. Mater.*, 2006, **18**, 5279-5288.
22. A. Zukal, I. Dominguez, J. Mayerova and J. Cejka, *Langmuir*,2009, **25**, 10314-10321.
23. J. H. Drese, S. Choi, R. P. Lively, W. J. Koros, D. J. Fauth, M. L. Gray and C. W. Jones, *Adv. Funct. Mater.*, 2009, **19**, 3821-3832.
24. D. Farrusseng, S. Aguado and C. Pinel, *Angew. Chem. Int. Ed.*, 2009, **48**, 7502-7513.
25. B. Liu, H. Shioyama, H. Jiang, X. Zhang and Q. Xu, *Carbon*, 2010, **48**, 456-463.
26. S. J. Yang, S. Nam, T. Kim, J. H. Im, H. Jung, J. H. Kang, S. Wi, B. Park and C. R. Park, *J. Am. Chem. Soc.*, 2013, **135**, 7394-7397.
27. J. Hafizovic, M. Bjørgen, U. Olsbye, P. D. Dietzel, S. Bordiga, C. Prestipino, C. Lamberti and K. P. Lillerud, *J. Am. Chem. Soc.*, 2007, **129**, 3612-3620.
28. M. Jahan, Q. Bao, J.-X. Yang and K. P. Loh, *J. Am. Chem. Soc.*, 2010, **132**, 14487-14495.
29. C. Petit and T. J. Bandosz, *J. Mater. Chem.*, 2009, **19**, 6521-6528.
30. M. Sabo, A. Henschel, H. Fröde, E. Klemm and S. Kaskel, *J. Mater. Chem.*, 2007, **17**, 3827-3832.
31. E. A. Fletcher, *Ind. Eng. Chem. Res.*, 1999, **38**, 2275-2282.
32 Y. Zheng, P. Li, H. Li and S. Chen, *Int. J. Electrochem. Sci.*, 2014, **9**, 7369-7381.
33. R. Fong, U. von Sacken and J. Dahn, *J. Electrochem. Soc.*, 1990, **137**, 2009-2013.
34. W. Lu and D. Chung, *Carbon*, 2001, **39**, 493-496.
35. E. Frackowiak and F. Beguin, *Carbon*, 2002, **40**, 1775-1787.
36. Y. A. Kim, M. Kojima, H. Muramatsu, S. Umemoto, T. Watanabe, K. Yoshida, K. Sato, T.

Ikeda, T. Hayashi and M. Endo, *Small*, 2006, **2**, 667-676.
37. G. Wu, C. Wang, X. Zhang, H. Yang, Z. Qi, P. He and W. Li, *J. Electrochem. Soc.*, 1999, **146**, 1696-1701.
38. B. Markovsky, M. D. Levi and D. Aurbach, *Electrochim. Acta*, 1998, **43**, 2287-2304.
39. Y.-P. Wu, C.-R. Wan, C.-Y. Jiang, S.-B. Fang and Y.-Y. Jiang, *Carbon*, 1999, **37**, 1901-1908.
40. T. Takamura, H. Awano, T. Ura and K. Sumiya, *J. Power Sources*, 1997, **68**, 114-119.
41. Y. Chen, X. Li, K. Park, J. Song, J. Hong, L. Zhou, Y.-W. Mai, H. Huang and J. B. Goodenough, *J. Am. Chem. Soc.*, 2013, **135**, 16280-16283.
42. S. Y. Chew, S. H. Ng, J. Wang, P. Novák, F. Krumeich, S. L. Chou, J. Chen and H. K. Liu, *Carbon*, 2009, **47**, 2976-2983
43. E. Yoo, J. Kim, E. Hosono, H. Zhou, T. Kudo and I. Honma, *Nano Lett.*, 2008, **8**, 2277-2282.
44. C. Li, X. Yin, L. Chen, Q. Li and T. Wang, *J. Phys. Chem. C*, 2009, **113**, 13438-13442.
45. Z.-S. Wu, W. Ren, L. Xu, F. Li and H.-M. Cheng, *ACS Nano*, 2011, **5**, 5463-5471.

Figure Caption

Scheme 1 Fabrication process of the 3D porous carbon materials.

Fig. 1 (a) SEM image, (b) EDS, (c) XRD pattern and (d) TGA curve of MOF-5.

Fig. 2 (a and b) SEM and (c and d) TEM images of 3D porous carbon derived from MOF-5.

Fig. 3 (a) EDS, (b) FTIR spectra, (c) XRD patterns, (d) Raman spectra and (e) N_2 adsorption-desorption isotherms of 3D porous carbon derived from MOF-5. Inset e is the pore size distribution calculated from the adsorption branch by the BJH model.

Fig. 4 (a) CV curves of the 3D porous carbon derived from MOF-5 electrode at 0.2 mV/s. (b) Galvanostatic charge/discharge profiles of 3D porous carbon derived from MOF-5 for the 1st, 2nd, and 100th cycling.

Fig. 5 (a) Cycling stability of 3D porous carbon derived from MOF-5 at a current density of 100 mA g^{-1}. (b) Rate performance of 3D porous carbon derived from MOF-5.

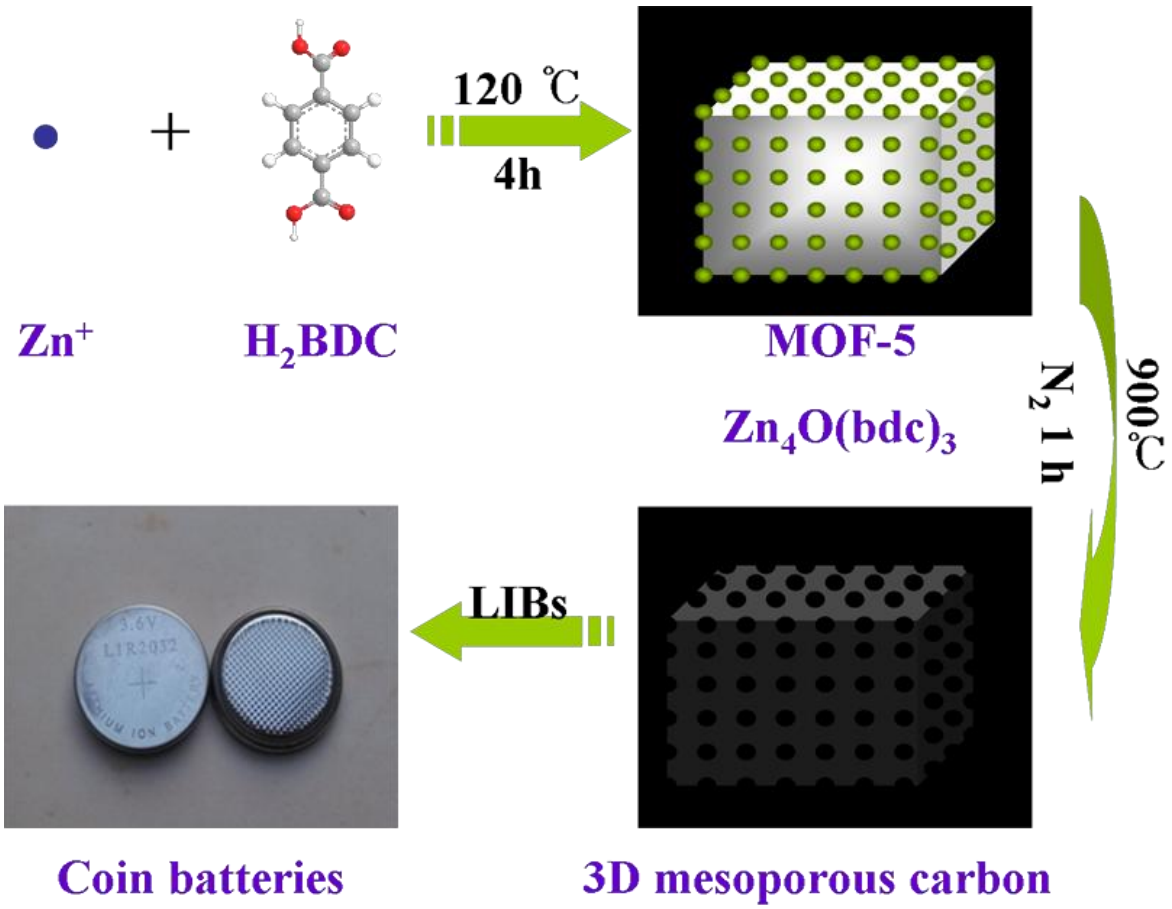

Scheme 1

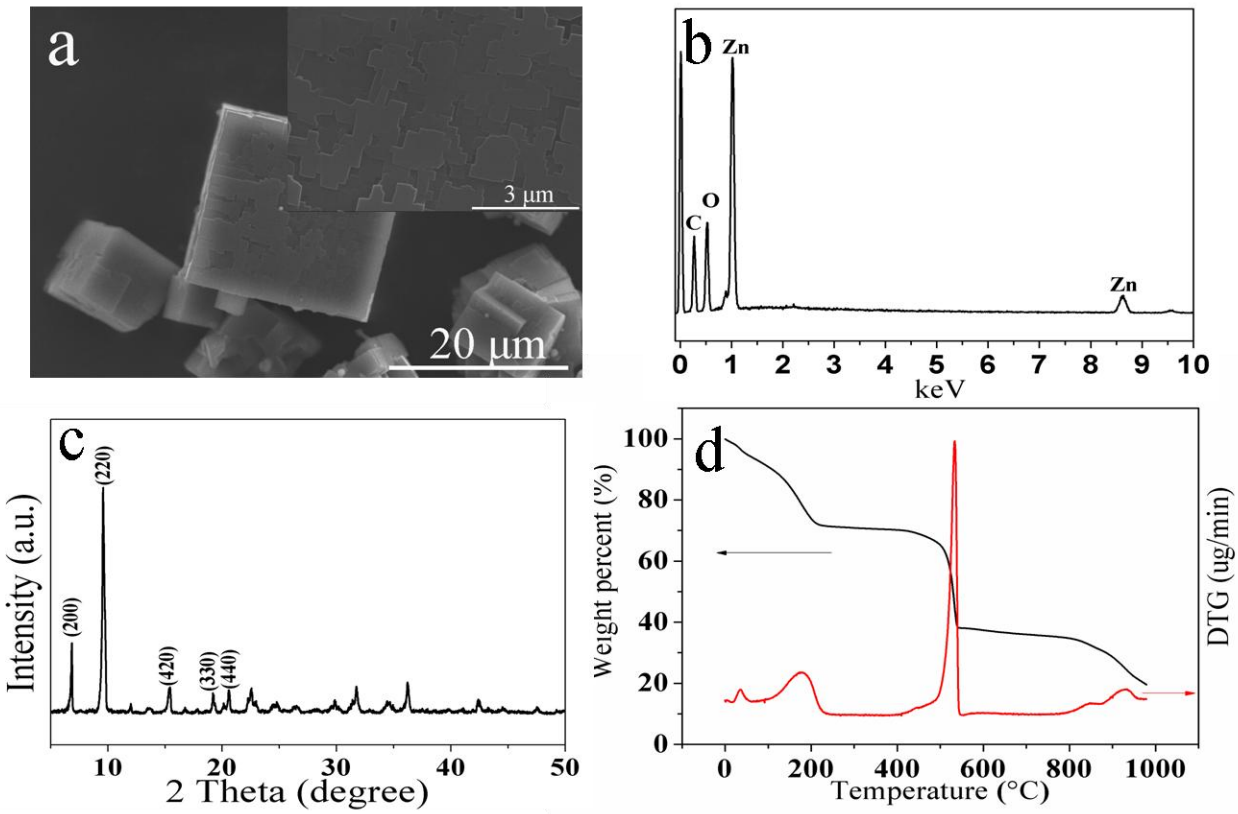

Fig. 1.

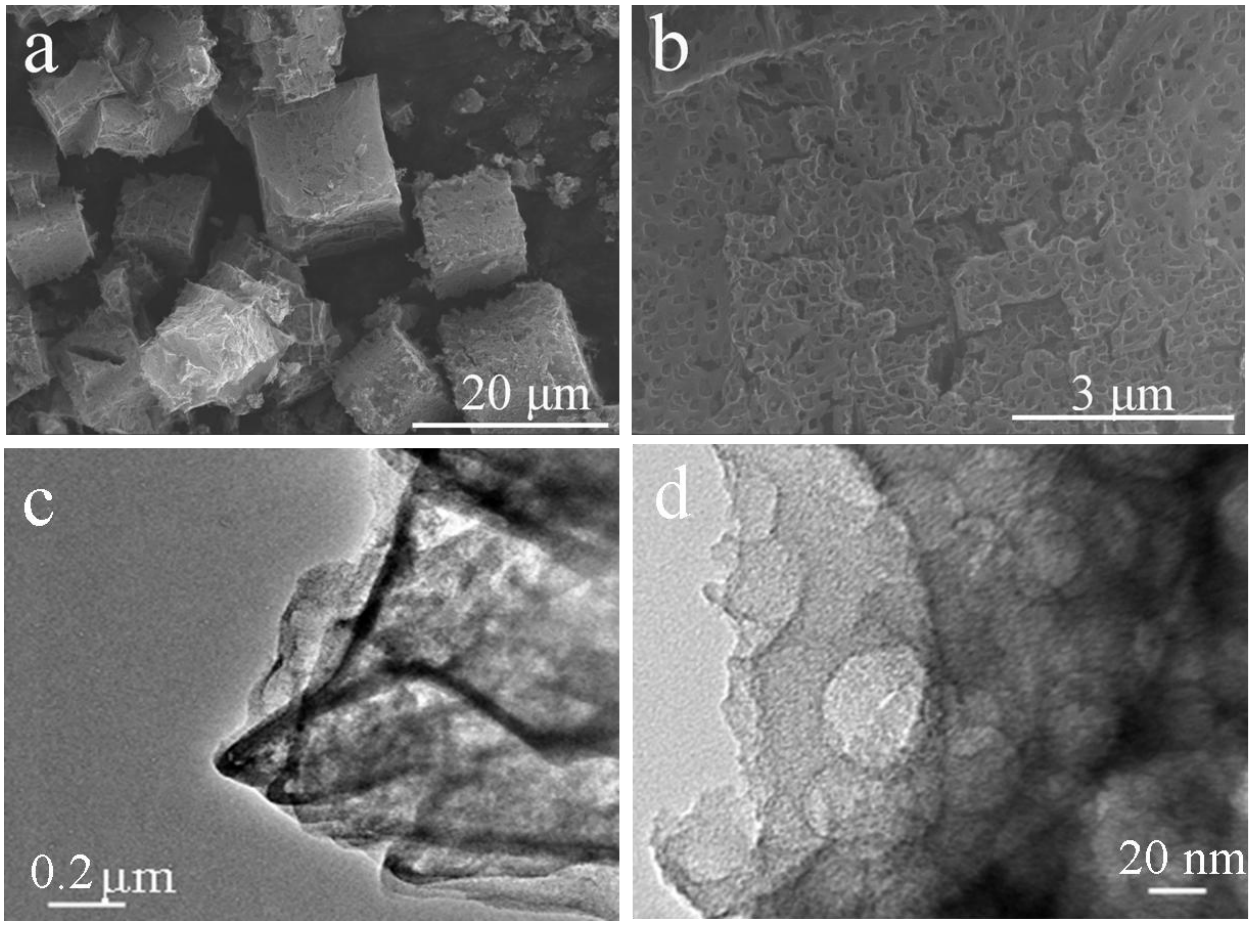

Fig. 2.

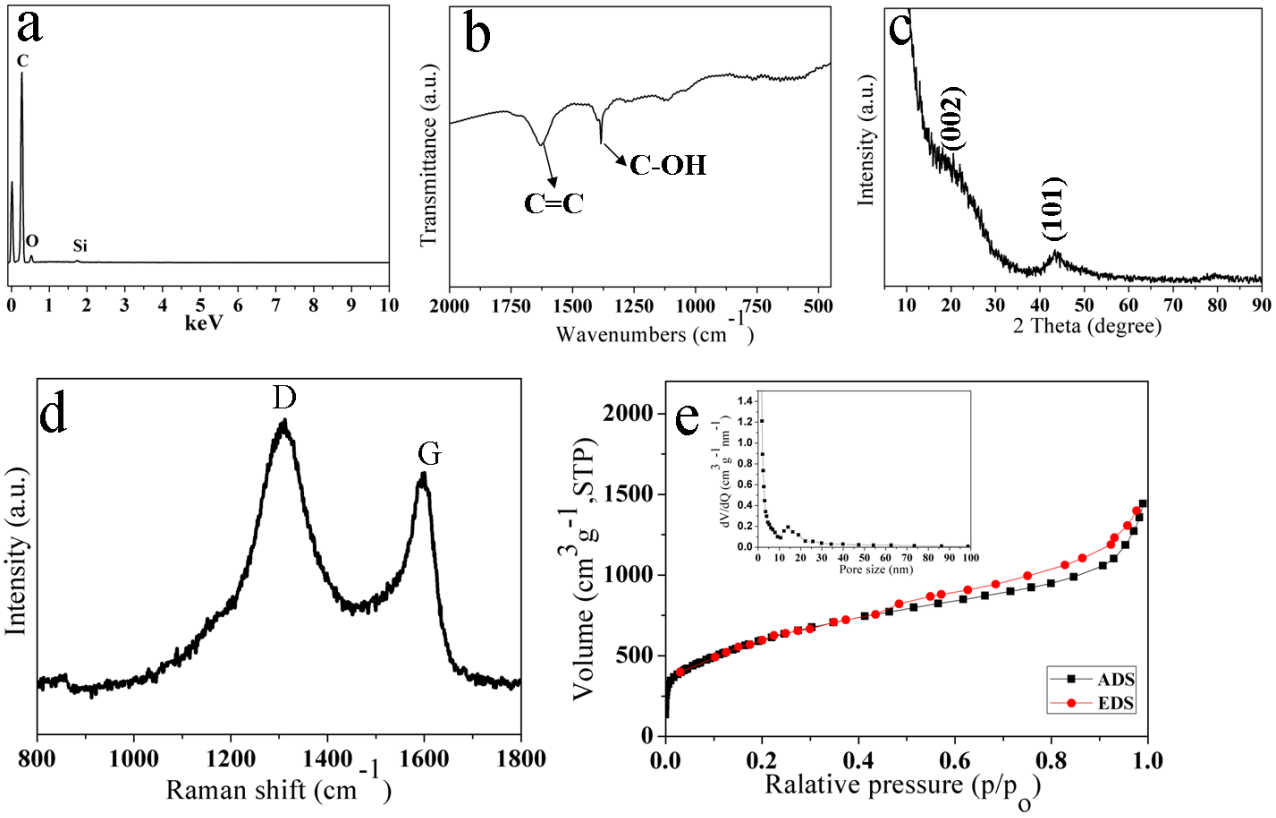

Fig. 3

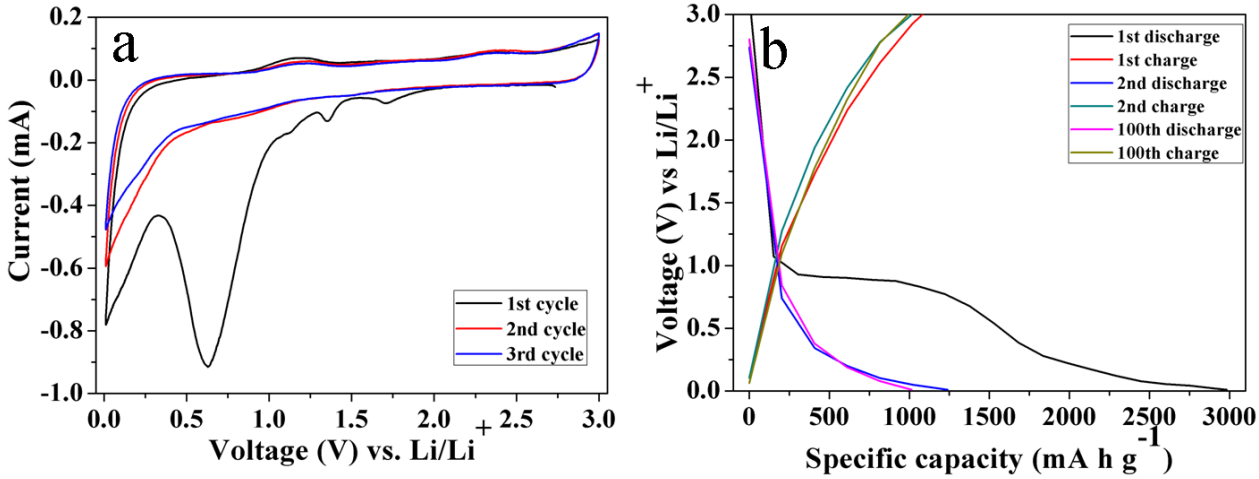

Fig. 4

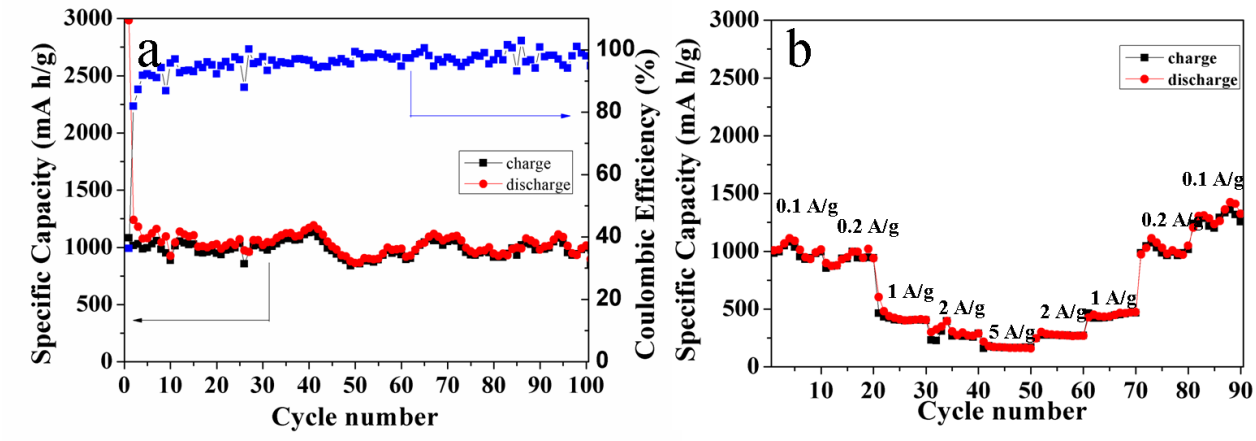

Fig. 5

Table 1. Comparison of the performance of similar materials as anode materials for lithium ion batteries.

Active material	BET surface area (m^2 g^{-1})	Current density mA g^{-1}	Initial capacity mA h g^{-1}	Capacity mA h g^{-1} (N^{th})	References
GNS[a] +C_{60}	-	50	784	600 (20)	43
Porous carbon	3315	50	2041	1000 (2)	23
CNFs[b]	74.5	200	631.9	400 (45)	44
B-doped graphene	256	50	2783	1327 (30)	45
N-doped graphene	290	50	2127	896 (30)	45
SWCNT[c]	657	25	2390	100 (40)	42
DWCNT[d]	583	25	2110	25 (40)	42
MWCNT[e]	55	25	750	250 (40)	42
CNTs[f]/CNFs	1840	100	~2458	~1150 (70)	41
Carbon coated ZnO	513	75	~2300	~1200 (50)	26
3D porous carbon	1880	100	2983	~1015 (100)	This work

[a] Graphene nanosheet [b] Carbon nanofibers [c] Single-wall carbon nanotube

[d] Double-wall carbon nanotube [e] Multi-wall carbon nanotube [f] Carbon nanotubes